Partner-assisted artificial selection of a secondary function for efficient bioremediation

Marco Zaccaria[1], Natalie Sandlin[1], Yoav Soen[2], and Babak Momeni[1,*]

[1] *Biology Department, Boston College, 140 Commonwealth Ave, Chestnut Hill, MA 02467 US*

[2] *Department of Biomolecular Sciences, Weizmann Institute of Science, 7670001 Rehovot, Israel*

* Corresponding author and lead contact, momeni@bc.edu

Summary

Microbial enzymes can address diverse challenges such as degradation of toxins. However, if the function of interest does not confer a sufficient fitness effect on the producer, the enzymatic function cannot be improved in the host cells by a conventional selection scheme. To overcome this limitation, we propose an alternative scheme, termed 'partner-assisted artificial selection' (PAAS), wherein the population of enzyme producers is assisted by function-dependent feedback from an accessory population. Simulations investigating the efficiency of toxin degradation reveal that this strategy supports selection of improved degradation performance, which is robust to stochasticity in the model parameters. We observe that conventional considerations still apply in PAAS: more restrictive bottlenecks lead to stronger selection but add uncertainty. Overall, we offer a guideline for successful implementation of PAAS and highlight its potentials and limitations.

Introduction

The vast diversity of bacterial and fungal enzymes offers potential solutions to many current challenges, including the removal of toxic compounds. Recycling complex compounds is an integrated part of the life-style for many bacteria and fungi. The same enzymes can potentially target and remove toxins that contaminate our food, water, and environment. One hurdle in employing native bacterial and fungal enzymes is that the function they are adapted for may not match the degradation of our toxins of interest. As a result, the detoxification performance will not meet the demands for practical applications. How can we improve such enzymatic functions? Selection for improved activity would be a clear choice, but what if enzymatic activity against such toxins is a secondary function, where toxin presence or degradation has no direct impact on the growth of bacterial or fungal cells that produce the enzyme?

An illustrative example is the bacterial degradation of mycotoxins—fungal produced food contaminants that are toxic to consume. There are several bacteria and fungi that have already been identified to carry enzymes that degrade mycotoxins [1–6]. However, at least in some cases, the presence of the toxin has little impact on the growth of bacterial cells, posing a challenge for selection. To show an example of such a situation, we have measured the growth rate of *Rhodococcus erythropolis* under different concentrations of aflatoxin G2 (AFG_2) in the culture (Fig S1). Even though *R. erythropolis* is known to degrade aflatoxins [7,8], AFG_2 has little positive

or negative impact on its growth rate.

To implement a selection scheme for improving secondary microbial functions, such as detoxification of AFG_2 by *Rhodococcus*, the detoxification performance should be linked to the detoxifier's growth properties. We propose adding an "assisting" partner population that provides the feedback from the toxin to the detoxifier (Fig 1). Community evolution has recently been revisited for its potential to improve community functions [9–11]. Here we take a slightly different approach by designing a community to select for a desired microbial function. We assume here that we have a library of variants with different quantitative traits, and our selection scheme favors variants with the best detoxification properties.

Results

Indirect selection of toxin degraders by interaction with an assisting population

We consider a scenario in which a toxin **T**, is degraded by a 'degrader' species **D**, but the toxin has little impact (positive or negative) on the growth properties of **D** cells. To enable selection of cells with improved detoxification efficiency, we introduce an assisting population, **A**, satisfying the following requirements (Fig 1, left): **A** is inhibited by **T** and provides a benefit to **D**, but the direct impact of **D** on **A** (i.e. in the absence of toxin) is negligible. Degradation of the toxin in coculture of **A** and **D**, alleviates growth inhibition of **A** thus increasing the positive influence of **A** on **D**. The positive feedback between **A** and **D** confers selective advantage of variants of **D** that better degrade **T**. In each round of the proposed selection scheme (Fig 1, right), the ancestral **A** is paired with evolved **D** from a previous round, thereby focusing the evolutionary pressure on **D**. The interaction with **A**, enables selection of the best-performing **D** variants at each round (Fig 1, right). Variation among different droplets arise from variations within the **D** population from previous rounds of selection as well as random mutations (either natural or induced). The benefit of exclusive propagation of the evolved **D** is two-fold: (1) Avoiding the acquisition of toxin resistance by **A** that would, in turn compromise the selection of improved degraders, and (2) simplifying the population dynamics by reverting to the ancestral population of **A** at the beginning of each cycle, relieving some of the anticipated restrictions on the scope of community evolution [12].

To assess the feasibility and potential efficiency of the selection scheme in Fig 1, we employed a population model (termed ImpInt) that accounts for the effects of **A** on **D**, **D** on **T**, and **T** on **A** (Methods-Model 1). These types of effects are likely applicable to diverse microbial systems (see Materials and Methods for more details and references). For simplicity, we assume that the rate of growth and carrying capacity of the assisting population **A** decrease with increasing concentration of the toxin **T** (consistent with [13–16]). We also assume that the rate of toxin degradation is proportional to the density of the degraders **D**, and that changes in toxin concentration lead to proportional changes in the growth rate and carrying capacity of **A** [17]. Fig. 2 provides an example for the simulated dynamics of **A**, **D** and **T**, starting with a given concentration of toxin and low densities of the populations **A** and **D** (compared their densities at carrying capacity). It demonstrates constant rate of growth of **A** accompanied by accelerated growth of **D** and reciprocal

decrease in the toxin concentration leading to its complete depletion before the populations **A** and **D** reach their saturation levels.

To assess the adequacy of the ImpInt model for analyzing the dynamics in this system, we compared the results of this model to the results of two additional models that explicitly incorporate, either the **T**-degrading enzyme produced by **D** (ExpEnz, Methods-Model 2), or the **A**-derived resource supporting the growth of **D** (ExpRes, Methods-Model 3). We found that the ImpInt model adequately approximates the dynamics of the more explicit ExpEnz and ExpRes models (Figs S2 and S3), except for the case of very strong enzymatic degradation of the toxin. For simulations outside the regime of strong degradation, we therefore used the simpler ImpInt model, whereas for simulations within this regime, one could use a modified implicit model (ImpLD, Methods-Model 4), in which the toxin is degraded only by growing **D** cells (Fig S4).

Geometric mean of A and D population sizes determines culture usability

We next sought to investigate the range of co-culture conditions permitting over 50% reduction of toxin concentration within the time scale of observation (direct derivation of conditions satisfying the toxin degradation criterion is provided in the Methods section). We found that the propensity to satisfy this condition increases with higher initial densities of **A** and **D** (Fig 3A) and that the geometric mean of the initial densities of **A** and **D** ($\sqrt{A_0 D_0}$) is a good predictor of the ability to degrade the toxin within a given time (Fig 3B). An initially high density of either of **A** or **D** can therefore compensate for low initial density of its partner.

Despite other sources of stochasticity, selection based on total cell density leads to improved detoxification

The main premise of our proposed PAAS scheme is that effective detoxification will be translated into improved overall culture growth (measured as the total cell density)—a trait that can be readily selected on. To assess the efficacy of such an approach, we computationally examined whether variants with better detoxification rates would be selected using PAAS. To create a more realistic situation, we assumed that in addition to the detoxification rate, other properties of the population (including their growth rates, carrying capacities, inhibition coefficient of **A** by **T**, and growth support coefficient of **D** by **A**) also varied stochastically (see Table 2). We then simulated many conditions (n=10000 instances) with random assignments of these variables and examined the traits in the output.

First, we found that the detoxification rate (d_D) showed a positive association with overall cell density, measured in total cell density (Fig 4A). Additionally, the overall detoxification performance was correlated with the total cell density, as expected (Fig 4B). To examine the efficacy of selection, we compared the distributions of the detoxification rates before selection and after selecting the top 10% instances with the highest total cell densities. This selection in PAAS clearly exhibits a preference for higher detoxification rates (Fig 4C). These results confirm the capability of PAAS to select for improved detoxifiers. Additionally, PAAS offers the advantage that cell density as the primary trait of interest is relatively easy to measure, compared to direct measurements of the toxin concentration, e.g. through fluorescence [18], ELISA, or HPLC [19,20].

Effective detoxification selection is sensitive to the timing of propagation

To assess the efficacy of the selection scheme, we used detox improvement as a measure of improvement in function, defined as the average detoxification rate of selected instances compared to that of initial instances. We first assessed how the initial composition of the coculture affected detox improvement. Interestingly, the selection performance—as estimated by detox improvement—was higher in a particular range of initial densities (Fig 5A). Further investigation revealed that this range corresponded to initial cell densities that resulted in **T** being mostly, but not completely, degraded. In fact, examining the data based on the residual **T** after 60 hours of simulated growth showed a clear trend with detox improvement being maximum around 1% residual **T** and dropping to lower values when residual **T** was much higher or lower (Fig 5B). This trend is intuitively expected; with too little or too much degradation, there is little information for resolving which cultures are performing well for degradation. We additionally examined the effect of the time between inoculation and passage and the results, consistent with the effect of initial density (Fig 5), that low, but not too low, residual **T** leads to the best detox improvement (Fig S5).

Detoxification selection depends on the population bottleneck

Selection is expected to depend on the size of the bottleneck. With a more stringent bottleneck (i.e. selecting more extreme cases), the expectation is to get more extreme phenotypes, but at the risk of added uncertainty of losing the best performers. We asked if the same considerations applied to the PAAS scheme. We constructed 100 samples of the PAAS scheme, with n = 100 instances of coculture (with stochastic parameters as in Table 2) in each of the samples. For each of these cases, we enforced a range of bottlenecks, from choosing the top 1% total cell density, to choosing the top 30%. The results showed that, as expected, the outcome of less stringent bottlenecks was more consistent, but on average led to lower improvement (Fig 6A). Defining *bottleneck stringency* as the fraction of the total number of instances to the instances selected, we saw a saturable improvement with more stringent bottlenecks (Fig 6B). Importantly, the uncertainty in detox improvement was directly related to how stringent the bottleneck was, with $\sigma_{bottleneck} = \sqrt{N_{bottleneck}}$, and $N_{bottleneck}$ as the size of the selected instances in the bottleneck (Fig 6C). Overall, these trends follow the expectations for a standard selection scheme.

Stochasticity in other cell traits can disrupt effective selection in PAAS

Stochasticity in other parameters is one of the main factors that can potentially derail the PAAS selection scheme by muddying which cultures are the best detoxifiers. We examined how different parameters correlated with the total cell density as our main selection criterion (Fig S6). We then asked how much stochasticity in other parameters can be tolerated in PAAS. For this, we examined a range of different values of standard deviations for the parameters listed in Table 2. We found that excessive stochasticity in other traits could mask the detoxification performance of the cocultures (Fig 7). This was evident as the correlation between detoxification rate and the total cell density (i.e. our criterion for selection) is lost when stochasticity in other traits is large (Fig 7A). As a result, our selection for improved detoxification is no longer effective in such cases (Fig 7B).

Discussion

We investigated the capabilities and limitations of a partner-assisted artificial selection scheme to select for functions of interest that have no significant impact on the growth properties of cells that provide them. We introduced an assisting population that created a feedback between the function of interest (e.g. degradation of a toxin) and the growth properties of the microbial cells that provide that function. To investigate the potentials and limits of PAAS, we examined a system consisting of a toxin degrader, along with an assisting population that was sensitive to the toxin of interest and beneficial to the degrader population. As a proxy for evolutionary dynamics, we examine how different variants fare in a single round of growth within a droplet. The choice of droplets as a platform limits the interactions between different variants of the evolving toxin degrader population. Additionally, the ability to choose best-performing droplets simplifies the overall selection scheme.

We found that selection for total cell density can lead to improved detoxification rates. This selection is most effective if it happens when detoxification is close to complete, so that there is enough discrimination between degraders with different performance. We see that bottleneck considerations in PAAS largely mirror our expectations in standard selection schemes. A more stringent bottleneck leads to a saturating improvement in detoxification performance, but at the cost of more uncertainty. Finally, we observe that too much stochasticity in other traits can mask the performance of toxin degradation and interfere with PAAS selection.

Do successive cycles of the proposed selection improve the detoxification performance? Answering this question will address whether assessing the performance in a single cycle is a reasonable proxy for the overall selection scheme. To answer this question, we simulated the process of successive cycles of selection, outlined in Fig 1: after each round of selection, we inoculated new droplets with the **D** cells selected from the best-performing droplets and ancestral **A** cells for another round of selection. The results suggest that these successive cycles lead to further improvement in detoxification, although the improvement slows down in later selection cycles (Fig S7). Importantly, how heritable the traits are will have a sizeable impact on the improvement in the following selection cycles because the randomness added on at the end of each cycle can undo some of the progress made towards better detoxification performance in previous rounds. As expected, when **A** and **D** evolve together, selection for **A**'s resistance to the toxin disrupts the selection for improved detoxification (Fig S8).

For practical implementation, we note that initial population sizes and the timing of selection can be used as effective design parameters. One major decision for designing an effective PAAS is the choice of bottleneck stringency; our *in silico* model suggests that PAAS is similar to a standard selection scheme in terms of how a more stringent bottleneck leads to stronger, but more uncertain, selection. Another major decision is the treatment of other sources of stochasticity. Among stochastic parameters that could interfere with selection, the growth rates of **A** and **D** appear to play major roles (Fig S6). Since the **A** population is reintroduced at the beginning of each round (Fig 1, right), a pre-adaptation step to maximize its growth rate can significantly reduce the variability in this trait. In contrast, the growth rate of **D**, as long as it does not come at the cost of loss of detoxification capabilities, could be considered a desired trait to select for.

Limitations of Study

In our treatment of different traits, we have assumed that such traits are independent of each other. However, some correlation between these traits is possible, for example a positive or negative correlation between the growth rate and carrying capacity of cells [21]. If known, such correlations can be directly incorporated into the model for a more realistic representation of stochasticity. As an example, we have included a tradeoff between the detoxification rate (d_D) and the carrying capacity (K_D) of population **D** to account for the possibility of better detoxification coming at a cost. This idea resembles the cost of providing a benefit by the associated microbes included in a model of host-microbe interactions put forward by van Vilet and Doebeli [22]. Our results suggest that our previous conclusions hold with a weak tradeoff, but a strong tradeoff can disrupt this selection scheme (Fig S9). The reason is that when d_D and K_D are strongly anticorrelated, best detoxifiers no longer correspond to the highest total cell density.

Some of the previous reports (e.g. Doulcier *et al.* [23] and Xie *et al.* [9]) have discussed the details of community composition and its role on selection. In our case, the trajectory of community dynamics appears insensitive to the details of the population composition (Fig S10). Therefore, we have not entered into detailed analysis of the impact of relative abundances on the outcome.

One of the assumptions in our model is that there is little direct impact on **A** by **D**, be it positive or negative. This can be controlled to some extent by choosing **A** that satisfies this assumption or by adjusting the resources in the environment. We expect results similar to the condition examined in this manuscript with weakly positive or negative impact on **A** by **D**. Strong positive or negative impact on **A** by **D** can change the community properties. Extreme exploitation conditions could drive **A** out of the community and disrupt PAAS. In contrast, strong mutualism is expected to stabilize the population dynamics [24] and lead to a more balanced performance regardless of the initial conditions.

The construction of PAAS communities is conceptually similar to the "Helper-Manufacturer" communities examined by Xie and colleagues [25] with one main difference: the Helper-Manufacturer system is based on commensalism, whereas the Assist-Detox system is based on mutualism. We believe some of the basic concepts and considerations for artificial selection, including those discussed in detail in [25], are shared between the two systems. However, for the specific goal of detoxification, the stronger bond between the partners in mutualism leads to stronger selection and expedites the process of finding improved detoxifiers.

Overall, we propose that PAAS can be utilized as an additional tool to expand the power of selection to situations where the function of interest has little influence on the growth properties of the provider of that function. We recognize that an actual implementation will likely involve adjusting the scheme to the specifics of a system of interest. Our simplified model presented in this work offers a baseline to build upon.

Acknowledgments

BM and MZ are supported by the National Science Foundation (NSF-CBET) under Grant No. 2103545. NS is supported by a NIFA-AFRI Predoctoral Fellowship from the USDA (Award No. 2021-67034-35108). YS was supported by the Sir John Templeton Foundation (grant numbers: 40663 and 764 61122). Figure 1 was created with BioRender.com.

Author Contributions

Marco Zaccaria: Conceptualization, Visualization, Writing- Reviewing and Editing. **Natalie Sandlin**: Conceptualization, Visualization, Writing- Reviewing and Editing. **Yoav Soen**: Methodology. Writing- Reviewing and Editing. **Babak Momeni**: Conceptualization, Methodology, Software, Data curation, Visualization, Writing- Original draft preparation, Writing- Reviewing and Editing.

Declaration of Interests

MZ, NS, and BM have a pending patent application related to this work.

Figure legends

Fig 1. An assisting population A can generate a positive feedback for D from the toxin T. The overall scheme and the specific requirements are shown on the left. On the right, a conceptual selection scheme is illustrated in which cycles of coculture (with ancestral **A** and evolved **D**) leads to improved detoxification performance of **D**. We envision a droplet-based implementation where **D** is clonal within each culture but different droplets contain different variants of **D**.

Fig 2. The assisting and degrading populations can grow together and degrade the toxin of interest. The dynamics of population densities (A) and the toxin concentration (B) are shown after incorporating all interactions. In the example shown here, populations **A** and **D** are assumed to be initially at 10^5 cells/ml and the initial toxin concentration is 10 μg/ml. All relevant parameters are listed in Table 1. The ImpInt model is used for this simulation.

Fig 3. Usability of A-D cocultures depend on the geometric mean of the initial A and D population densities. (A) Surveying a range of initial **A** and **D** population densities shows that an increase in the initial density of one can compensate for a drop in the initial density of the other one to maintain usability for toxin removal. (B) Examining the final **T** concentrations suggest that the geometric mean of the initial **A** and **D** population densities is the main determinant of usability and detoxification performance. Final **T** concentrations are taken from the simulations at 72 hours.

In all cases the initial toxin concentration is 10 μg/ml. All relevant parameters are listed in Table 1. The ImpInt model is used in these simulations.

Fig 4. A survey of many (n=10000) simulated instances with stochastic parameters shows that PAAS allows us to select for improved detoxification as a secondary function. (A) Scatter-plot of all instances shows a positive correlation between the detoxification rate and total cell density. The red trend line is estimated based on the average total cell densities at low and high detox rates. (B) Total cell density is also tightly linked to the effectiveness of detoxification. (C) Comparing the distributions of the detoxification rates before selection and after selecting the top 10% instances with the highest total cell densities shows that PAAS favors improved detoxification. Final **T** concentrations are taken from the simulations at 46 hours. In all cases the initial toxin concentration is 10 μg/ml. All relevant parameters are listed in Table 1 and stochastic properties are listed in Table 2. The ImpInt model is used in these simulations.

Fig 5. For optimal selection, most, but not all, of the toxin should be degraded at the time of selection. (A) Mean detox improvement (defined as the average of detoxification rates at the end of a round divided by its initial value) is plotted as a function of initial population densities of **A** and **D**. (B) Mean detox improvement data in (A) is plotted as a function of the final residual **T**, showing an optimal performance around 1% residual **T** at the end of each round. For each data point, 1000 instances were sampled, with stochastic parameters listed in Table 2. Final **T** concentrations are taken from the simulations at 60 hours. In all cases the initial toxin concentration is 10 μg/ml. All relevant parameters are listed in Tables 1 and 2. The ImpInt model is used in these simulations.

Fig 6. Improvement in detox, as a function of population bottleneck. (A) The distribution of detox improvement values is shown when different fractions of the top cases with the highest cell density are selected within a round. More stringent selections can potentially yield higher detox improvement, but at the risk of more uncertainty. (B) Error bars are standard deviations (n = 100). Red curve is a fit into the data, with the form $y = 1 + (y_f - 1)\, x/(x + x_s)$, where $y_f = 1.3$ and $x_s = 5$. (C) Red curve is a linear fit into the data, $y = mx$, where $m = 2.7$. Final **T** concentrations are taken from the simulations at 72 hours. In all cases the initial toxin concentration is 10 μg/ml. All relevant parameters are listed in Table 1. The ImpInt model is used in these simulations.

Fig 7. Stochasticity in other traits can interfere with PAAS efficiency. (A) Correlation between total cell density and detoxification rate decreases as stochasticity in other traits increases. Correlation coefficient is calculated using all instances of cocultures with parameters picked from corresponding random variables. Stochasticity is defined as the ratio of σ to μ (see Table 2) and the same value is used for all random variables except $\mathbf{d_D}$ for which σ/μ is fixed at 0.2. Error bars are standard deviations calculated using the top 10% of instances selected based on total cell

density. (B) Detox improvement decreases with more stochasticity in other traits. Here, error bars depict bootstrap 95% confidence intervals using 100 samples of PAAS. Top 10% of the instances with the largest total population densities are selected for calculating detox improvement. All relevant parameters are similar to Fig 4 and listed in Tables 1. The ImpInt model is used in these simulations.

STAR Methods

Resource Availability

Lead Contact

Further information and requests for resources and codes should be directed to and will be fulfilled by the lead contact, Babak Momeni (momeni@bc.edu).

Materials availability

This study did not generate new unique reagents.

Data and code availability

- Growth rate characterization data reported in this paper will be shared by the lead contact upon request.
- All original codes have been deposited at Zenodo and are publicly available as of the date of publication. DOIs are listed in the key resources table.
- Any additional information required to reanalyze the data reported in this paper is available from the lead contact upon request.

Method Details

Bacterial growth characterization

Rhodococcus erythropolis (DSM 43066) was grown from the frozen stock in glucose-yeast-malt (GYM) at 28° C with continuous shaking (240 rpm) for 24 hrs before starting the experiments. For the growth characterization experiment, *R. erythropolis* was cultured in basal Z medium: KH_2PO_4 (1.5 g/L), K_2HPO_4 x $3H_2O$ (3.8 g/L), $(NH_4)_2SO_4$ (1.3 g/L), sodium citrate dihydrate (3.0g/L), $FeSO_4$ (1.1 mg/L), glucose (4.0 g/L), 100x vitamin solution (1 mL), 1000x trace elements solution (1 mL), 1 M $MgCl_2$ (5 mL), 1 M $CaCl_2$ (1 mL), and 100x amino acid stock (10 mL). AFG_2 stock (Cayman Chemical) was dissolved in LC-MS grade methanol to the final concentration of 1 mg/mL. AFG_2 was then introduced into the growth cultures at different concentrations by further diluting the stock in methanol to keep the total methanol concentration fixed across all cases.

Final volumes of 150 µl per well were used in standard flat-bottom 96-well plates. A BioTek Synergy Mx multi-mode microplate reader was used to monitor optical density of cells at 600 nm. Reads were taken at 5 min intervals over 48 hrs. Cultures usually started at an initial OD of 0.01 and were continuously shaking between reads. Five replicates were used per condition. Only the

internal wells of the 96-well plate were used for samples, and the peripheral wells of the plate were filled with sterile water to contain evaporation.

Growth rates were calculated using a Matlab code that extracted the data from text files generated by BioTek Synergy Mx. The function `'fit_logistic'` (written by James Condor, and available at https://www.mathworks.com/matlabcentral/fileexchange/41781-fit_logistic-t-q) was used to estimate the growth rates from OD readings.

Models and equations

There are three assumptions shared in our models. (1) The growth rate of assisting population **A** linearly decreases as the **T** concentration increases [16]. (2) The growth rate of **A** and its carrying capacity proportionally change at different concentrations of an inhibitor [17]. This trend is observed in other studies, for example in the response of *Salmonella* to tetracycline [13,14], response of *E. coli* to streptomycin [13], and response of *Acetobacter* to acetic acid [15]. (3) Detoxification rate of **T** is proportional to the density of the detoxifying population **D**.

For the first assumption, there are numerous examples that show the decrease in growth rate at higher concentrations of an inhibitor. A few examples are shown in the Supplementary Information of Ref. [21], such as the response of *Staphylococcus aureus* to acetic acid and erythromycin and the response of *Escherichia coli* to various antibiotics. The biological justification of this relationship is that cell inhibition mechanisms often slow down basic cellular processes such as DNA replication or protein synthesis machinery and thus decrease the growth rate.

Regarding the second assumption, in addition to the impact of toxins on the growth rate of species, cells have to invest more energy and resources to undo the harmful effects of the inhibitor (e.g. produce more DNA polymerase, produce more ribosomes, or activate efflux pumps to excrete the toxin). This additional investment reduces the overall resources available to the cell and thus leads to a lower carrying capacity when more toxins are present. In Ref. [17], this trend is quantitatively shown for several bacterial isolates from the human nasal passage. This trend is also observed in other studies, for example in the response of *Salmonella* to tetracycline [13,14], response of *E. coli* to streptomycin [13], and response of *Acetobacter* to acetic acid [15].

For the third assumption, regardless of the exact details of the detoxification mechanism, it is expected that with more **D** cells the detoxification will proportionally increase. There could be exceptions to this assumption when for example quorum sensing affects **D**'s response, or when crowding reduces the overall performance. Nonetheless, the baseline assumption, which is expected to apply in the majority of cases is that total detoxification per unit time is proportional to the density of **D** cells.

To capture the main features proposed in our model, it suffices that both growth rate and carrying capacity decrease at higher **T** concentrations. Nonetheless, we have made more specific assumptions in our model based on known properties that are both realistic and simple to represent.

Model 1: Implicit interaction effects (ImpInt)

In this simplified model, we assume logistic growth for the **A** and **D** populations. The toxin **T** is assumed to modulate both the growth rate and the carrying capacity of the population **A**. Growth

rate and carrying capacity of population **D** is capped by the benefits supplied by population **A**.

$$\frac{dA}{dt} = (r_A - \rho_T T)\left(1 - \frac{A}{K_A(1-\rho_T T/r_A)}\right)A \quad (1)$$

$$\frac{dD}{dt} = min(r_D, s_A A)\left(1 - \frac{D}{AK_D/K_A}\right)D \quad (2)$$

$$\frac{dT}{dt} = -d_D DT \quad (3)$$

Here D and A are the densities of **A** and **D** populations, respectively, and T is the concentration of the toxin **T**. In Eq. (2), the maximum growth rate is presented as $min(r_D, s_A A)$. This choice is made to cap the growth rate to the intrinsic maximum growth rate, r_D, which prevents the unrealistically high values of population growth rate when the support supplied by **A** is abundant. The motivation is that under such a situation the overall growth rate of **D** will be limited by another bottleneck such as the time required for duplicating the DNA. The same form of equations is used in the following in Model 2 and Model 4.

Model 2: Explicit enzyme effect (ExpEnz)

In this model, the **T**-degrading enzyme (produced by **D**) is explicitly included. Compared to ImpInt, rather than direct detoxification of **T** by **D**, **D** produces the enzyme E which degrades **T**. We have also included an explicit term for intrinsic enzyme decay in our equations.

$$\frac{dA}{dt} = (r_A - \rho_T T)\left(1 - \frac{A}{K_A(1-\rho_T T/r_A)}\right)A \quad (4)$$

$$\frac{dD}{dt} = min(r_D, s_A A)\left(1 - \frac{D}{AK_D/K_A}\right)D \quad (5)$$

$$\frac{dE}{dt} = \eta_D D\left(1 - \frac{D}{\gamma A}\right) - \delta_E E \quad (6)$$

$$\frac{dT}{dt} = -d_E ET \quad (7)$$

Model 3: Explicit resource effect (ExpRes)

In this model, the resource **R**, produced by **A** and supporting the growth of **D**, is explicitly included. We assume a standard Monod-type growth for **D** on **R** as its main limiting resource. The consumption of **R** by **D** is also assumed to be proportional to the biomass generated by the growing **D** population.

$$\frac{dA}{dt} = (r_A - \rho_T T)\left(1 - \frac{A}{K_A(1-\rho_T T/r_A)}\right)A \quad (8)$$

$$\frac{dR}{dt} = \beta_R \frac{dA}{dt} - \alpha_D\left(\frac{R}{R+K_R}\right)D \quad (9)$$

$$\frac{dD}{dt} = r_D\left(\frac{R}{R+K_R}\right)D \quad (10)$$

$$\frac{dT}{dt} = -d_D DT \quad (11)$$

Model 4: Implicit interaction effects, live degradation (ImpLD)

In this modified phenomenological model, we assume that only growing **D** populations contribute to the detoxification. This will capture cases where the enzyme decay is large and thus detoxification stops when there is no growth and enzyme production by **D** cells.

$$\frac{dA}{dt} = (r_A - \rho_T T)\left(1 - \frac{A}{K_A(1-\rho_T T/r_A)}\right)A \quad (12)$$

$$\frac{dD}{dt} = min(r_D, s_A A)\left(1 - \frac{D}{AK_D/K_A}\right)D \quad (13)$$

$$\frac{dT}{dt} = -d_D D\left(1 - \frac{D}{AK_D/K_A}\right)T \quad (14)$$

Simulations

Numerical simulations were performed using MATLAB. Source codes along with descriptions of parameters are available at https://github.com/bmomeni/partner-assisted-artificial-selection. (cross-referenced at https://doi.org/10.5281/zenodo.8041025)

Parameters and their values

Unless otherwise stated, Table 1 lists the values of parameters used in our simulations. The order-of-magnitude of values are inferred from experimental characterization of aflatoxin G2 detoxification by *Rhodococcus* species.

Random variables

Table 2 lists the distributions used for different random variables used to include stochasticity in our simulations. For all normal random variables, we used the built-in `random` function in Matlab, with relevant parameters (e.g. `'uniform'` for a uniform distribution and `'normal'` for a normal distribution). To generate skew normal distributions for growth rates, we used the following transformation based on two independent random variables x_1 and x_2 picked from a Normal distribution $\mathcal{N}(0,1)$.

$$x_{sn} = \frac{\alpha|x_1|+x_2}{\sqrt{1+\alpha^2}} \quad (15)$$

Here α is the skew parameter in the distribution. The distribution is more skewed towards small (/large) values, when α is negative (/positive).

Quantifications and statistical analysis

Bootstrap confidence intervals are calculated using the `bootci` function in Matlab, with `mean` as the target function.

Estimated time for detoxification

To assess usability, we need to calculate if within the span of our observations there is a significant drop in the toxin concentration. We limit our discussions to weak detoxification cases here, because only such cases are relevant for the determination of usability within the observation time

t_{obs}. Additionally, we assume that D and A (densities of **A** and **D** populations, respectively) are away from their respective carrying capacities in these conditions, and that the growth of **D** is limited by the support of **A**. Thus, the equations will be simplified to

$$\frac{dA}{dt} \approx (r_A - \rho_T T)A \tag{16}$$

$$\frac{dD}{dt} = s_A AD \tag{17}$$

$$\frac{dT}{dt} = -d_D DT \tag{18}$$

We further approximate $(r_A - \rho_T T)$ as $(r_A - \rho_T T_0)$ during this time, with the assumption that the decrease in T is small in cases that are marginally viable. Therefore,

$$A(t) \approx A_0 \exp[(r_A - \rho_T T_0)t] \approx A_0[1 + (r_A - \rho_T T_0)t] \tag{19}$$

Then

$$\frac{dD}{dt} \approx s_A D A_0[1 + (r_A - \rho_T T_0)t]$$

$$\frac{d}{dt}\ln(D) \approx s_A A_0[1 + (r_A - \rho_T T_0)t]$$

$$D(t) \approx D_0 \exp\left[s_A A_0 \left(t + \tfrac{1}{2}(r_A - \rho_T T_0)t^2\right)\right] \tag{20}$$

Since we assume that changes in D are small within the observed time-scale t_{obs}, we thus get

$$D(t) \approx D_0 \left[1 + s_A A_0 \left(t + \tfrac{1}{2}(r_A - \rho_T T_0)t^2\right)\right] \tag{21}$$

Using this estimate, we can calculate T as

$$\frac{1}{T}\frac{dT}{dt} = -d_D D_0 \left[1 + s_A A_0 t + \frac{1}{2} s_A A_0 (r_A - \rho_T T_0)t^2\right]$$

$$\frac{d}{dt}\ln(T) = -d_D D_0 \left[1 + s_A A_0 t + \frac{1}{2} s_A A_0 (r_A - \rho_T T_0)t^2\right]$$

$$T(t) = T_0 \exp\left\{-d_D D_0 \left[t + \tfrac{1}{2} s_A A_0 t^2 + \tfrac{1}{6} s_A A_0 (r_A - \rho_T T_0)t^3\right]\right\} \tag{22}$$

The threshold for the culture to be functional (i.e. at least 50% detoxification) is

$$\frac{T(t_{obs})}{T_0} = \exp\left\{-d_D D_0 \left[t_{obs} + \frac{1}{2} s_A A_0 {t_{obs}}^2 + \frac{1}{6} s_A A_0 (r_A - \rho_T T_0){t_{obs}}^3\right]\right\} < 0.5$$

$$d_D D_0 \left[t_{obs} + \frac{1}{2} s_A A_0 {t_{obs}}^2 + \frac{1}{6} s_A A_0 (r_A - \rho_T T_0){t_{obs}}^3\right] > 0.69$$

$$\tfrac{1}{6} s_A A_0 (r_A - \rho_T T_0){t_{obs}}^3 + \tfrac{1}{6} s_A A_0 {t_{obs}}^2 + t_{obs} - \tfrac{0.69}{d_D D_0} > 0 \tag{23}$$

With $(r_A - \rho_T T_0) > 0$ this third-degree polynomial is monotonic, with a single positive solution for t_{obs}. If $(r_A - \rho_T T_0) < 0$, the first-order derivative of this third-degree polynomial has one positive and one negative zeros, and since the value of the function is negative at $t_{obs} = 0$, again there will be a single positive solution for t_{obs}.

Deriving the conditions for usability

Starting from the equations for ImpInt,

$$\frac{dA}{dt} = (r_A - \rho_T T)\left(1 - \frac{A}{K_A(1 - \rho_T T/r_A)}\right)A$$

$$\frac{dD}{dt} = min(r_D, s_A A)\left(1 - \frac{D}{A\,K_D/K_A}\right)D$$

$$\frac{dT}{dt} = -d_D DT$$

We focus on conditions that would determine the minimum requirements for usability. We note that if the observation time is long enough, all cultures will be viable in this formulation (the fixed point has *A* and *D* at their saturation densities and *T* at zero). A more realistic representation is obtained if we add an explicit death rate (δ) for population decline in the absence of growth.

$$\frac{dA}{dt} = (r_A - \rho_T T)\left(1 - \frac{A}{K_A(1-\rho_T T/r_A)}\right)A - \delta A \qquad (24)$$

$$\frac{dD}{dt} = min(r_D, s_A A)\left(1 - \frac{D}{AK_D/K_A}\right)D - \delta D \qquad (25)$$

$$\frac{dT}{dt} = -d_D DT \qquad (26)$$

We separate the analysis into three regimes (Fig S10):

(1) $r_A - \rho_T T_0 > 0$ and small δ

In this regime, the **A** population will exponentially increase from the beginning. In turn, the **D** population will increase with an increasing rate. From Eq. (23), we find that for usability, it is sufficient if $\min\left\{\frac{1}{6}s_A A_0(r_A - \rho_T T_0){t_{obs}}^3, \frac{1}{6}s_A A_0 {t_{obs}}^2, t_{obs}\right\} > \frac{0.69}{d_D D_0}$. This confirms our intuition that usability is achieved if the observation time is large enough, the initial detoxification by **D** is fast enough, or **A** adequately supports the growth of **D**.

(2) $r_A - \rho_T T_0 > 0$ and large δ

In this regime, the **A** population will slowly grow but the culture is viable only if the growth can support the growth of **D** before it goes extinct. The time-scale for decay of *D* (i.e. δ) becomes critical in this case and the system is expected to be viable if **A** grows rapidly enough within the time span of $t_e = 1/\delta \ln(D_0/D_{ext})$, where D_{ext} is the extinction density for population *D*. This will be satisfied if $s_A A_0 \exp[(r_A - \rho_T T - \delta)t_e] > \delta$ or in other terms when $s_A A_0 \exp\left[\frac{r_A - \rho_T T - \delta}{\delta}\ln(D_0/D_{ext})\right] > \delta$

(3) $r_A - \rho_T T_0 < 0$

In this regime, the **A** population will decline and can only be rescued if detoxification by **D** is rapid enough. The time-scale for decay of A is approximately $1/(\rho_T T_0 - r_A + \delta)$ and the system is expected to be viable if either $\ln(2)/min(r_D, s_A A) < 1/(\rho_T T_0 - r_A + \delta)$ (i.e. the doubling time of **D** is short) or $1/d_D D_0 < 1/(\rho_T T_0 - r_A + \delta)$ (i.e. detoxification happens rapidly).

Tables

Table 1. Typical parameter values for the model.

Parameter	Description	Value
t_f	Total simulation time per round	60 hr
r_A	Maximum growth rate of population **A**	0.2 hr^{-1}
r_D	Maximum growth rate of population **D**	0.22 hr^{-1}
K_A	Maximum carrying capacity of population **A**	10^8 cells/ml
K_D	Maximum carrying capacity of population **D**	3×10^8 cells/ml
ρ_T	Inhibition coefficient of **T** against **A**	0.003 ml/(μg·hr)
s_A	Growth coefficient of **A** in supporting **D**	10^{-7} ml/(cells·hr)
d_D	Detoxification rate of **T** removal by **D**	10^{-8} ml/(cells·hr)
d_E	Detoxification rate of **T** removal by **E**	10^{-8} ml/(U·hr)
η_D	Production rate of enzyme **E** by **D**	2.5×10^{-6} μU/(cells·ml)
β_R	Production rate of resource **R** by **A**	0.2 fmole/(cells·hr)
K_R	Monod coefficient for growth of **D** on **R**	0.2 μM
α_D	Consumption rate of resource **R** by **D**	0.07 fmole/cell
δ_E	Decay rate of enzyme **E**	0.02-0.5 hr^{-1}

Table 2. Different random variables and their distributions in a typical artificial selection simulation.

Random variable	Distribution	Value
$\mathbf{r_A}$	Skew-normal	$\mu = r_A$; σ =0.02r_A; skew α = -3
$\mathbf{r_D}$	Skew-normal	$\mu = r_D$; σ =0.02r_D; skew α = -3
$\mathbf{K_A}$	Normal	$\mu = K_A$; σ =0.02K_A
$\mathbf{K_D}$	Normal	$\mu = K_D$; σ =0.02K_D
$\boldsymbol{\rho_T}$	Normal	$\mu = \rho_T$; σ =0.02ρ_T
$\mathbf{s_A}$	Normal	$\mu = s_A$; σ =0.02s_A
$\mathbf{d_D}$	Normal	$\mu = d_D$; $\sigma = 0.2d_D$

References

1. Abatenh, E., Gizaw, B., Tsegaye, Z., and Wassie, M. (2017). The Role of Microorganisms in Bioremediation- A Review. Open Journal of Environmental Biology *2*, 038–046. 10.17352/ojeb.000007.

2. Wang, X., Qin, X., Hao, Z., Luo, H., Yao, B., and Su, X. (2019). Degradation of Four Major Mycotoxins by Eight Manganese Peroxidases in Presence of a Dicarboxylic Acid. Toxins 2019, Vol. 11, Page 566 *11*, 566. 10.3390/TOXINS11100566.

3. Wang, J., and Xie, Y. (2020). Review on microbial degradation of zearalenone and aflatoxins. Grain & Oil Science and Technology *3*, 117–125. 10.1016/J.GAOST.2020.05.002.

4. Adebo, O.A., Njobeh, P.B., Gbashi, S., Nwinyi, O.C., and Mavumengwana, V. (2017). Review on microbial degradation of aflatoxins. Crit Rev Food Sci Nutr *57*, 3208–3217. 10.1080/10408398.2015.1106440.

5. Ben Taheur, F., Kouidhi, B., Al Qurashi, Y.M.A., Ben Salah-Abbès, J., and Chaieb, K. (2019). Review: Biotechnology of mycotoxins detoxification using microorganisms and enzymes. Toxicon *160*, 12–22. 10.1016/j.toxicon.2019.02.001.

6. Sandlin, N., Russell Kish, D., Kim, J., Zaccaria, M., and Momeni, B. (2021). Current and emerging tools of computational biology to improve the detoxification of mycotoxins. Appl Environ Microbiol. 10.1128/AEM.02102-21.

7. Alberts, J., Engelbrecht, Y., Steyn, P., Holzapfel, W., and Zyl, Van, W. (2006). Biological degradation of aflatoxin B1 by Rhodococcus erythropolis cultures. Int J Food Microbiol *109*, 121–126. 10.1016/j.ijfoodmicro.2006.01.019.

8. Cserháti, M., Kriszt, B., Krifaton, Cs., Szoboszlay, S., Háhn, J., Tóth, Sz., Nagy, I., and Kukolya, J. (2013). Mycotoxin-degradation profile of Rhodococcus strains. Int J Food Microbiol *166*, 176–185. 10.1016/j.ijfoodmicro.2013.06.002.

9. Xie, L., Yuan, A.E., and Shou, W. (2019). Simulations reveal challenges to artificial community selection and possible strategies for success. PLoS Biol *17*, e3000295. 10.1371/JOURNAL.PBIO.3000295.

10. Xie, L., and Shou, W. (2021). Steering ecological-evolutionary dynamics to improve artificial selection of microbial communities. Nature Communications 2021 12:1 *12*, 1–15. 10.1038/s41467-021-26647-4.

11. Sánchez, Á., Vila, J.C.C., Chang, C.Y., Diaz-Colunga, J., Estrela, S., and Rebolleda-Gomez, M. (2021). Directed Evolution of Microbial Communities. https://doi.org/10.1146/annurev-biophys-101220-072829 *50*, 323–341. 10.1146/ANNUREV-BIOPHYS-101220-072829.

12. Chang, C.Y., Vila, J.C.C., Bender, M., Li, R., Mankowski, M.C., Bassette, M., Borden, J., Golfier, S., Sanchez, P.G.L., Waymack, R., et al. (2021). Engineering complex communities by directed evolution. Nature Ecology & Evolution 2021 5:7 *5*, 1011–1023. 10.1038/s41559-021-01457-5.

13. Hou, Z., An, Y., Hjort, K., Hjort, K., Sandegren, L., and Wu, Z. (2014). Time lapse investigation of antibiotic susceptibility using a microfluidic linear gradient 3D culture device. Lab Chip *14*, 3409–3418. 10.1039/C4LC00451E.

14. Brunelle, B.W., Bearson, S.M.D., and Bearson, B.L. (2013). Tetracycline accelerates the temporally-regulated invasion response in specific isolates of multidrug-resistant Salmonella

enterica serovar Typhimurium. BMC Microbiol *13*, 1–9. 10.1186/1471-2180-13-202/TABLES/2.

15. Chang, Y.C., Reddy, M.V., Imura, K., Onodera, R., Kamada, N., and Sano, Y. (2021). Two-Stage Polyhydroxyalkanoates (PHA) Production from Cheese Whey Using Acetobacter pasteurianus C1 and Bacillus sp. CYR1. Bioengineering 2021, Vol. 8, Page 157 *8*, 157. 10.3390/BIOENGINEERING8110157.

16. Niehaus, L., Boland, I., Liu, M., Chen, K., Fu, D., Henckel, C., Chaung, K., Miranda, S.E., Dyckman, S., Crum, M., et al. (2019). Microbial coexistence through chemical-mediated interactions. Nat Commun *10*, 2052. 10.1038/s41467-019-10062-x.

17. Dedrick, S., Warrier, V., Lemon, K.P., and Momeni, B. (2022). When does a Lotka-Volterra model represent microbial interactions? Insights from in-vitro nasal bacterial communities. bioRxiv, 2022.08.08.503228. 10.1101/2022.08.08.503228.

18. Zaccaria, M., Dawson, W., Kish, D.R., Reverberi, M., Bonaccorsi Di Patti, M.C., Domin, M., Cristiglio, V., Dellafiora, L., Gabel, F., Nakajima, T., et al. (2021). Mechanistic Insight from Full Quantum Mechanical Modeling: Laccase as a Detoxifier of Aflatoxins. bioRxiv, 2020.12.31.424992. 10.1101/2020.12.31.424992.

19. Rodríguez Velasco, M.L., Calonge Delso, M.M., and Ordónez Escudero, D. (2010). ELISA and HPLC determination of the occurrence of aflatoxin M 1 in raw cow's milk. http://dx.doi.org/10.1080/0265203021000045208 *20*, 276–280. 10.1080/0265203021000045208.

20. Alshannaq, A., and Yu, J.H. (2017). Occurrence, toxicity, and analysis of major mycotoxins in food. Int J Environ Res Public Health *14*. 10.3390/ijerph14060632.

21. Lipson, D.A. (2015). The complex relationship between microbial growth rate and yield and its implications for ecosystem processes. Front Microbiol *6*, 615. 10.3389/fmicb.2015.00615.

22. van Vliet, S., and Doebeli, M. (2019). The role of multilevel selection in host microbiome evolution. Proc Natl Acad Sci U S A *116*, 20591–20597. 10.1073/PNAS.1909790116/SUPPL_FILE/PNAS.1909790116.SAPP.PDF.

23. Doulcier, G., Lambert, A., De Monte, S., and Rainey, P.B. (2020). Eco-evolutionary dynamics of nested darwinian populations and the emergence of community-level heredity. Elife *9*, 1–40. 10.7554/ELIFE.53433.

24. Momeni, B., Brileya, K.A., Fields, M.W., Shou, W., Brileya, K.A., Fields, M.W., and Shou, W. (2013). Strong inter-population cooperation leads to partner intermixing in microbial communities. Elife *2*, e00230. 10.7554/eLife.00230.

25. Xie, L., Yuan, A.E., and Id, W.S. (2019). Simulations reveal challenges to artificial community selection and possible strategies for success. PLoS Biol *17*, e3000295. 10.1371/JOURNAL.PBIO.3000295.

Supplemental Figures

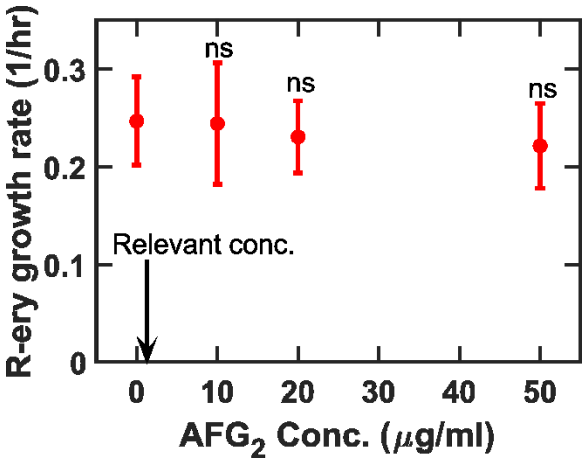

Figure S1. Growth rate of detoxifying strains such as *Rhodococcus erythropolis* is minimally affected by the presence of aflatoxins, highlighting the challenge of natural selection for improved detoxification, related to Figure 1. Different concentrations of AFG_2 (dissolved in methanol) are added to basal Z culture medium (see Materials and Methods, Bacterial growth characterization) inoculated with *R. erythropolis* at an initial cell OD of 0.01. Cultures are allowed to grow and the initial growth rate of *R. erythropolis* is estimated from the increase in OD over time (as a proxy for cell density). None of the growth rates at 10, 20, or 50 μg/ml of AFG_2 were statistically different from the no-toxin control (t test, $p>0.3$). For comparison, the upper limit of practically relevant concentrations of AFG_2 (around 1 μg/ml) is marked by an arrow as a point of reference to show that even at much higher AFG_2 concentrations the impact on growth rate of *R. erythropolis* populations is minimal.

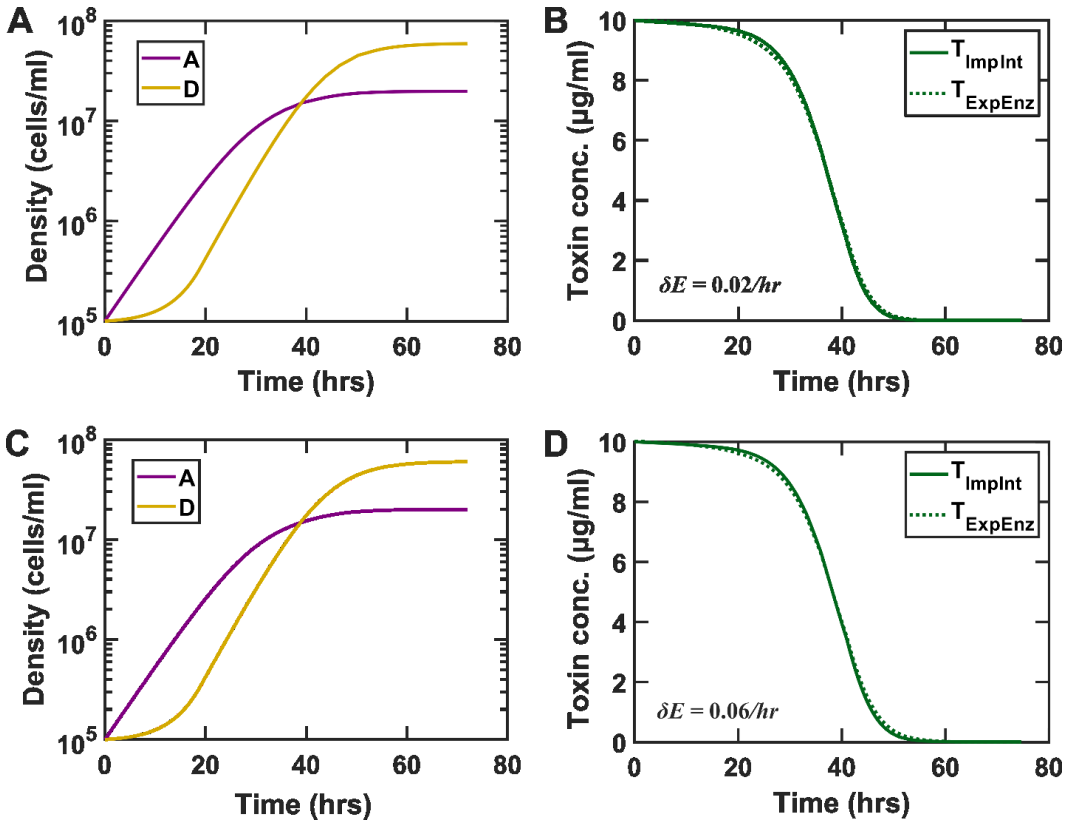

Figure S2. The simplified ImpInt model can adequately approximate a more mechanistic model that explicitly includes the degrading enzyme (ExpEnz), related to Figure 2. A.) Population dynamics of **A** and **D** using the ExpEnz model matches the ImpInt model at a relatively low enzymatic detoxification rate of δE = 0.02/hr. B.) The temporal variations of the toxin follow a similar trend in both ExpEnz and ImpInt models (δE = 0.02/hr). C.) Population dynamics of **A** and **D** using the ExpEnz model matches the ImpInt model at a intermediate enzymatic detoxification rate of δE = 0.06/hr. D.) The temporal variations of the toxin follow a similar trend in both ExpEnz and ImpInt models (δE = 0.06/hr). The equations behind ImpInt and ExpEnz models can be found in the Methods section (Model 1 and Model 2, respectively). The detoxification rate in ImpInt is adjusted to match the dynamics of **T** offered by ExpEnz.

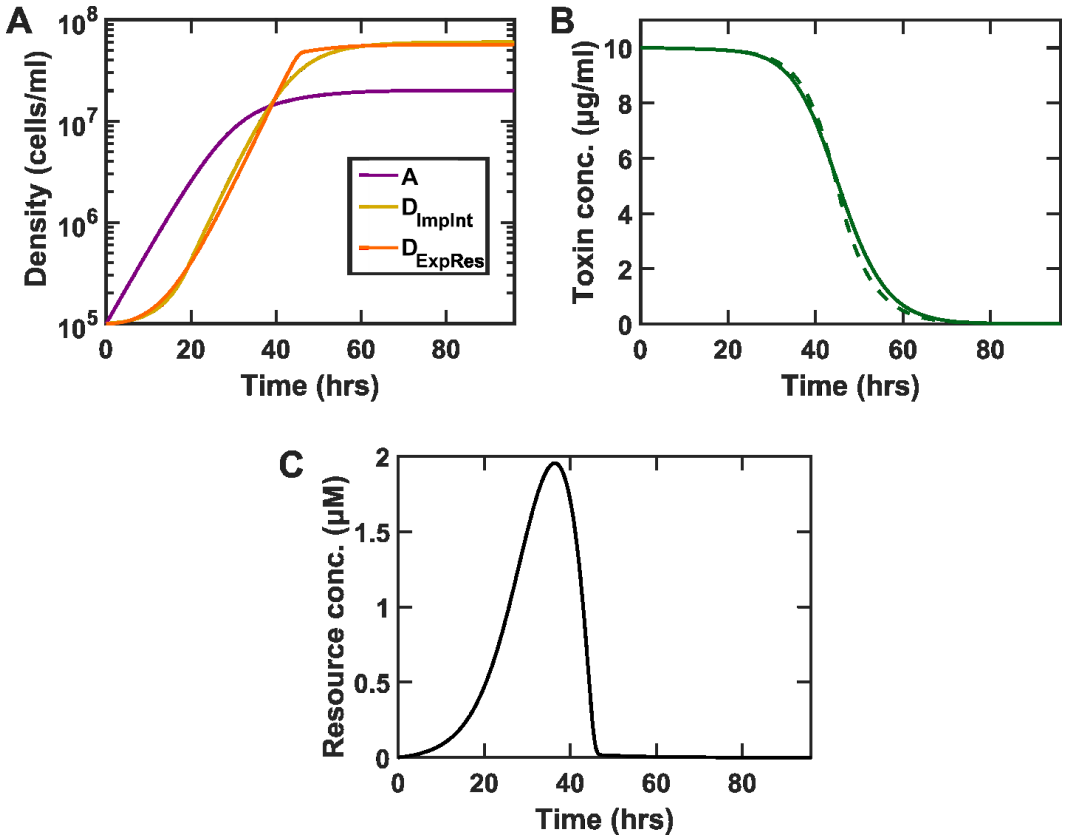

Figure S3. The simplified ImpInt model can adequately approximate a more mechanistic model that explicitly includes the resource or metabolite that mediates how population A supports population D (ExpRes), related to Figure 2. A.) Population dynamics of **A** and **D** using the ExpRes model qualitatively matches the ImpInt model. B.) The temporal variations of the toxin follow a similar trend in both ExpRes and ImpInt models. C.) Production and depletion of the resource produced by **A** and consumed by **D** is shown. The equations behind ImpInt and ExpRes models can be found in the Methods section (Model 1 and Model 3, respectively). The detoxification rate in ImpInt is adjusted to match the dynamics of **T** offered by ExpRes.

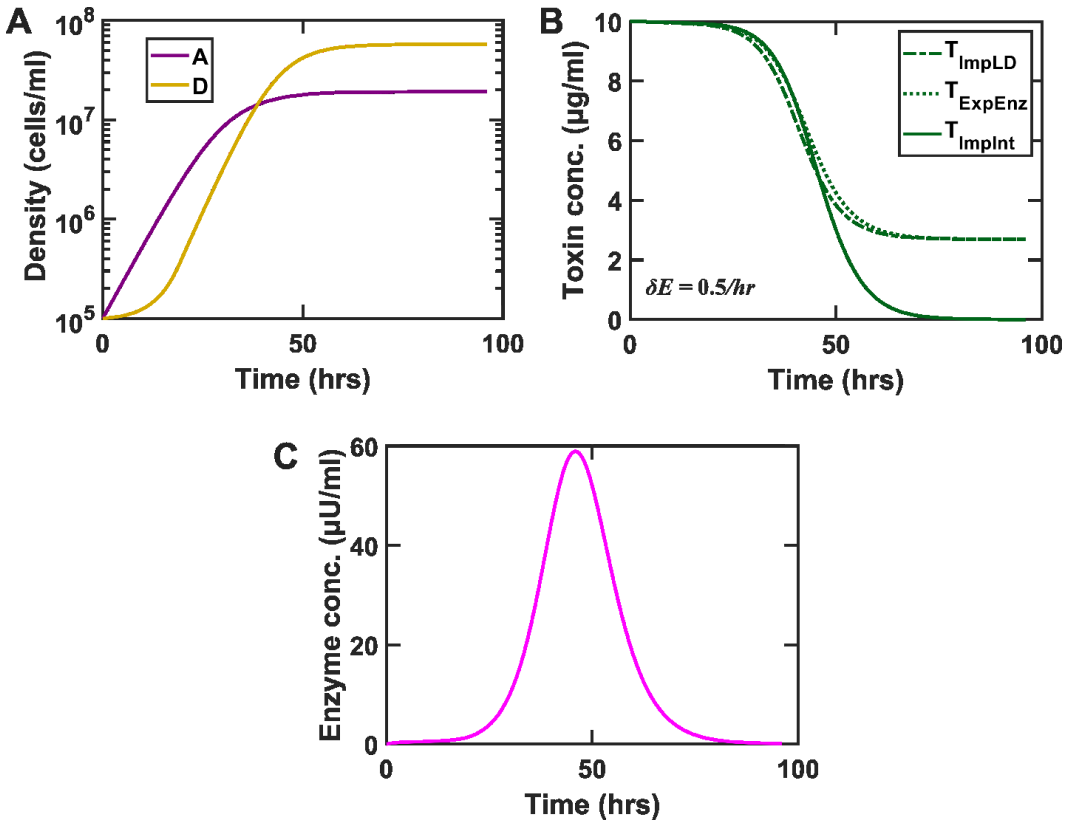

Figure S4. When enzyme decay rate is large, a modified implicit model that assumes detoxification only by growing D cells (ImpLD) can adequately approximate the model that explicitly includes the degrading enzyme (ExpEnz), related to Figure 2. A.) Population dynamics of **A** and **D** using the ExpRes model qualitatively matches the ImpLD model. B.) The temporal variations of the toxin follow a similar trend in both ExpEnz and ImpLD models. C.) Temporal profile of the enzyme concentration in the ExpEnz model is shown. The equations behind ImpLD and ExpEnz models can be found in the Methods section (Model 4 and Model 2, respectively). The detoxification rate in ImpLD is adjusted to match the dynamics of **T** offered by ExpEnz. We note that ImpInt no longer matches the dynamics of **T** from ExpEnz when the enzyme decay rate is very high.

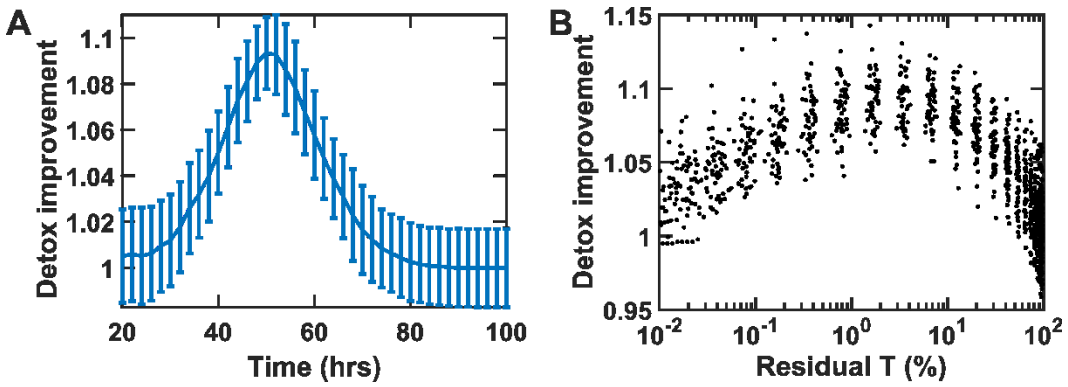

Figure S5. For optimal selection, most, but not all, of the toxin should be degraded at the time of selection, related to Figure 5. A.) Detox improvement (defined as the average of detoxification rate at the end of a round divided by its initial value) is plotted as a function of detoxification time. Error bars show standard deviations calculated among 50 independent instances. B.) Detox improvement data in (A) is plotted as a function of the final residual T, showing an optimal performance around 1% residual **T** at the end of each round. For each data point, 1000 instances were sampled, with stochastic parameters listed in Table 2. Initial **A** and **D** densities are 10^5 cells/ml each. In all cases the initial toxin concentration is 10 μg/ml. All relevant parameters are listed in Tables 1 and 2, except $K_A = 2\times10^7$ cells/ml and $K_D = 6\times10^7$ cells/ml. The ImpInt model is used in these simulations. All the parameters match those in Fig 5.

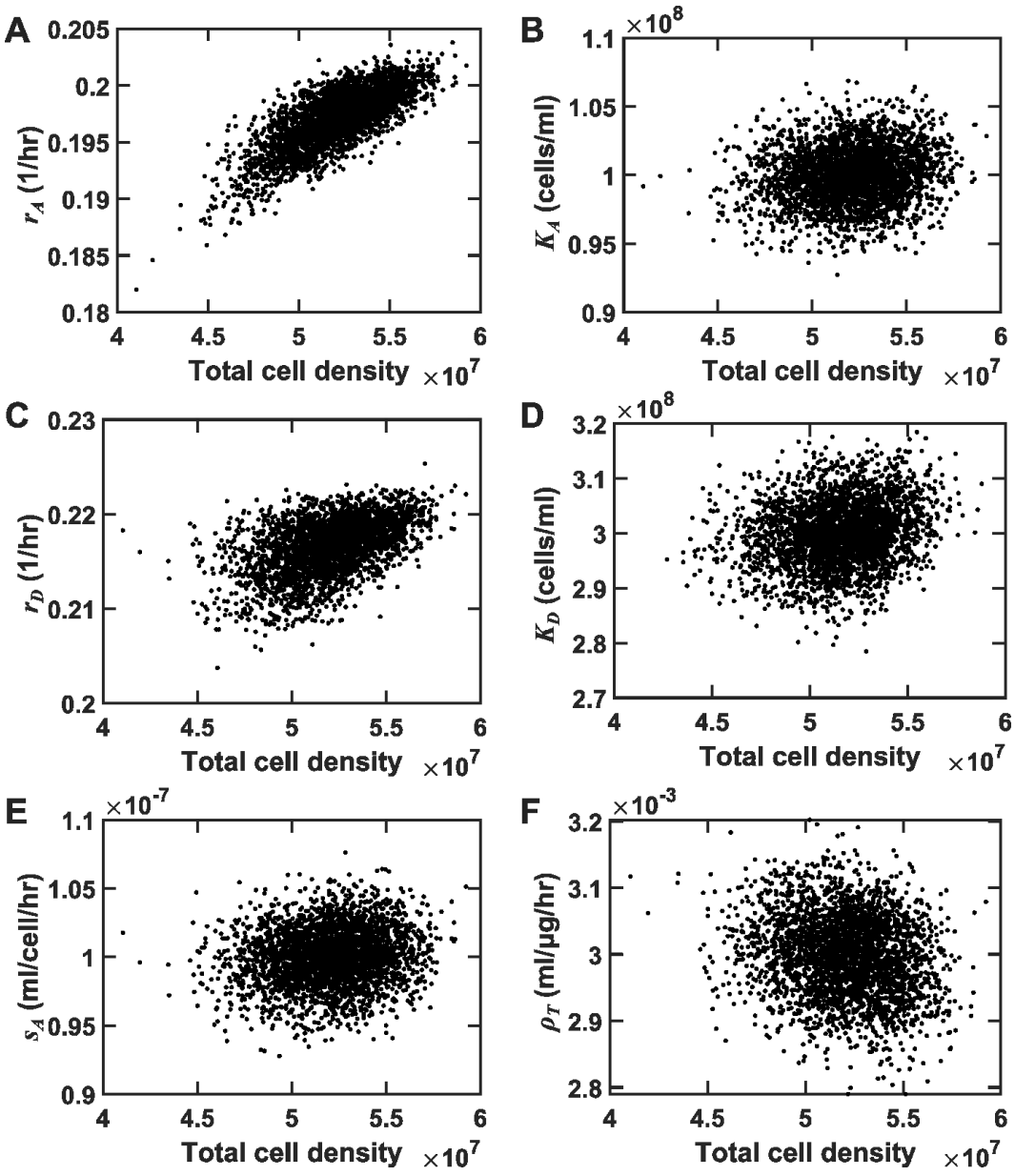

Figure S6. Stochasticity in growth rates of A and D as the major contributors to the total cell density can interfere with detoxification selection, related to Figure 7. We survey n=3000 simulated instances with stochastic parameters to evaluate how stochasticity in parameters affects PAAS selection. In scatter plots, total cell density in each instance is plotted with respect to one of the following phenotypic parameters. A.) Growth rate of **A**. B.) Carrying capacity of **A**. C.) Growth rate of **D**. D.) Carrying capacity of **D**. E.) Growth coefficient of **A** in support of **D**. F.) Inhibition coefficient of **T** against **A**. Scatter-plots show that among different parameters, r_A and r_D are the most influential in determining the total cell, and can thus interfere with our ability to select for improved detoxification. Total cell density is found from simulations at 46 hours. The initial toxin concentration is 10 μg/ml. All relevant parameters are listed in Table 1 and stochastic properties are listed in Table 2. The ImpInt model is used in these simulations.

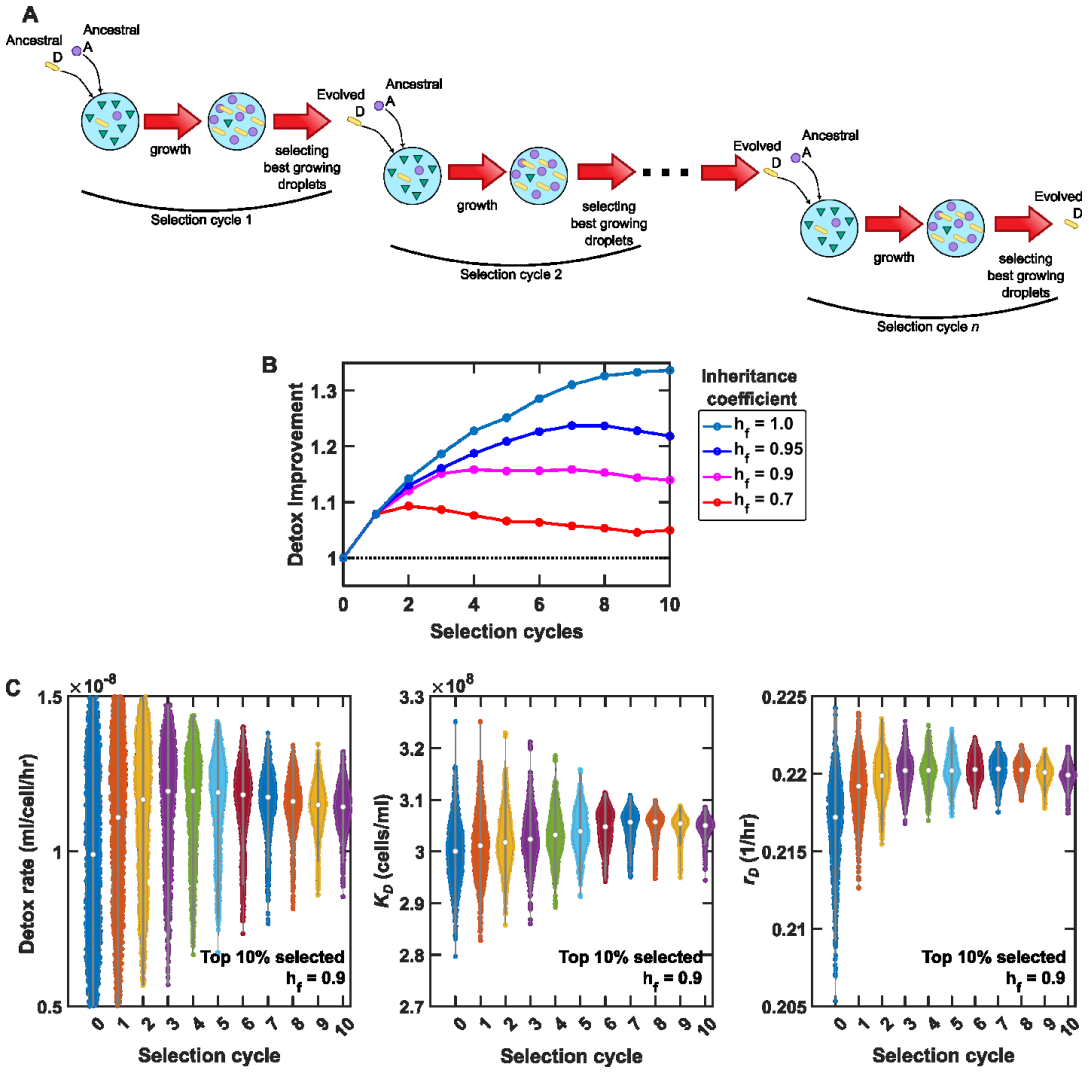

Figure S7. Successive rounds of selection can lead to improved detoxification, related to Figure 7. We survey n=10000 simulated droplets in each cycle, starting from an initial population of **A** and **D** with random properties listed in Tables 1 and 2. Within each cycle, we simulate the growth of culture inside droplets with an initial toxin concentration T_0 = 10 μg/ml. At 48 hours, we select the top 10% of the droplets that have the highest total populations densities (**A**+**D**). From these droplets, evolved **D** is separated from **A** and is mixed with ancestral **A** to inoculate the next cycle of selection. A.), the entirety of the process is schematically shown. B.) We calculated 'detox improvement' (the average of detoxification rates at the end of a cycle divided by its average value in the ancestral population) over different selection cycles. We assumed that the properties of **D** cells are mainly driven by inheritance, but are also affected by random or induced variations. Mathematically, $x_{inoc,i} = h_f \cdot x_{final,i-1} + (1 - h_f) \cdot x_{inoc,0}$, where $x_{inoc,i}$ is the random variable corresponding to any property of **D** cells inoculating droplets in the selection cycle i and $x_{final,i}$ is the random variable corresponding to that property after the selection cycle i. We observe that successive selection shows diminishing returns but still can improve the detoxification. This benefit is weaker when the inheritance coefficient is smaller. C.) By examining the distribution of different traits of **D** over successive cycles, we note that selection for the carrying capacity of **D** limits the improvement of detoxification rates. Nevertheless, improvements in growth properties of **D** (r_D and K_D) and improvements in the detox rate (d_D) lead to improved overall detoxification performance. The lmplnt model is used in these simulations.

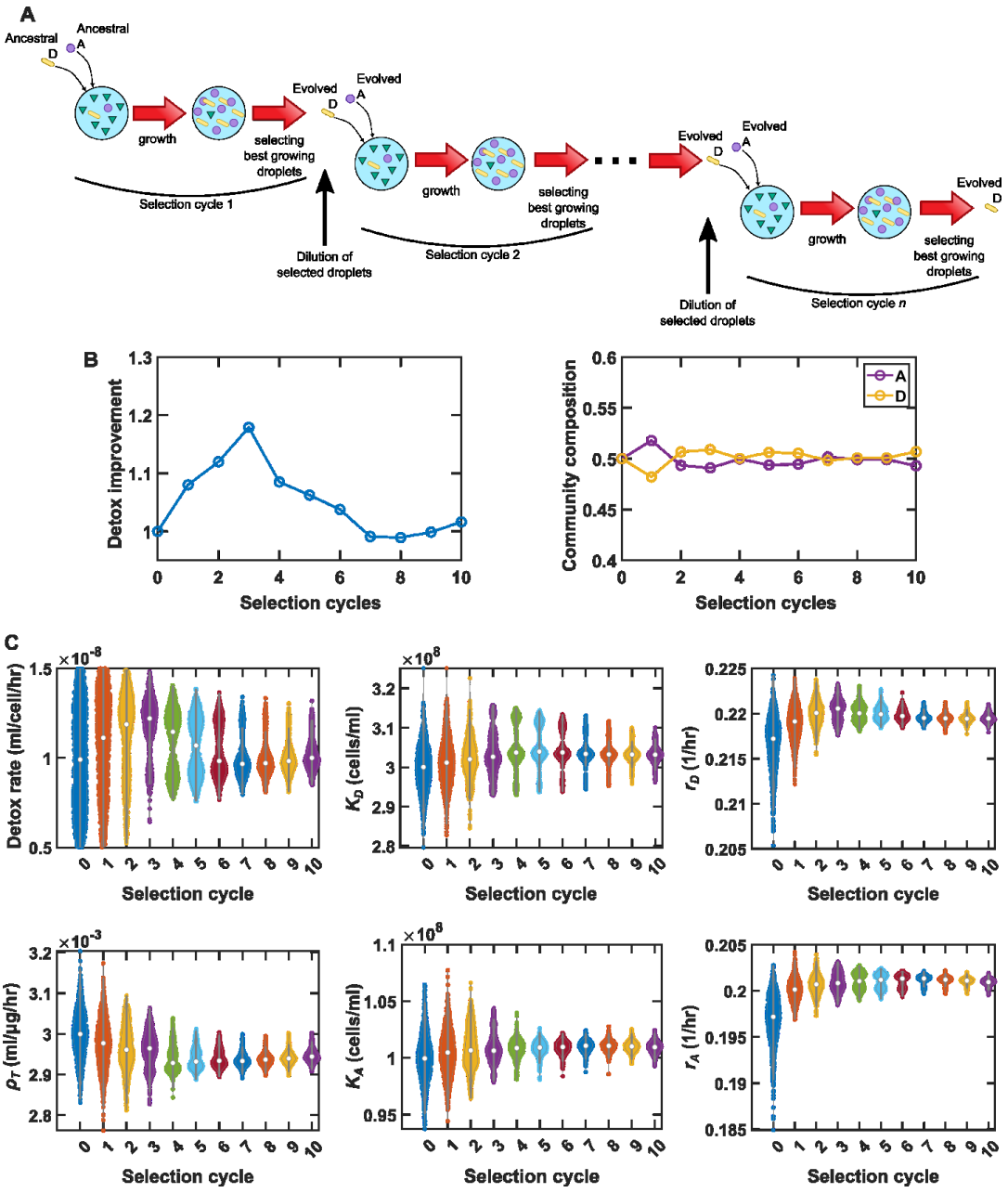

Figure S8. When A and D evolve together, selection for A's resistance to the toxin disrupts the selections of improved detoxification, related to Figure 7. We survey n=10000 simulated droplets in each cycle, starting from an initial population of **A** and **D** with random properties listed in Tables 1 and 2. Within each cycle, we simulate the growth of culture inside droplets with an initial toxin concentration T_0 = 10 µg/ml. At 48 hours, we select the top 10% of the droplets that have the highest total populations densities (**A**+**D**). From these droplets, evolved **D** and evolved **A** cells are used to inoculate the next cycle of selection. A.) The entirety of the process is schematically shown. B.) We calculated 'detox improvement' as well as changes in the population composition at the end of each selection cycle. In these simulations, $h_f = 0.9$. We observe that selection for more resistance of **A** to the toxin (lower ρ_T) reverts the improvement in detoxification (higher d_D). C.) By examining the distribution of different traits of **D** and **A** over successive cycles, we note that the lineage with more resistance to the toxin outcompetes and replaces the lineage with better detoxification rate. The Implnt model is used in these simulations.

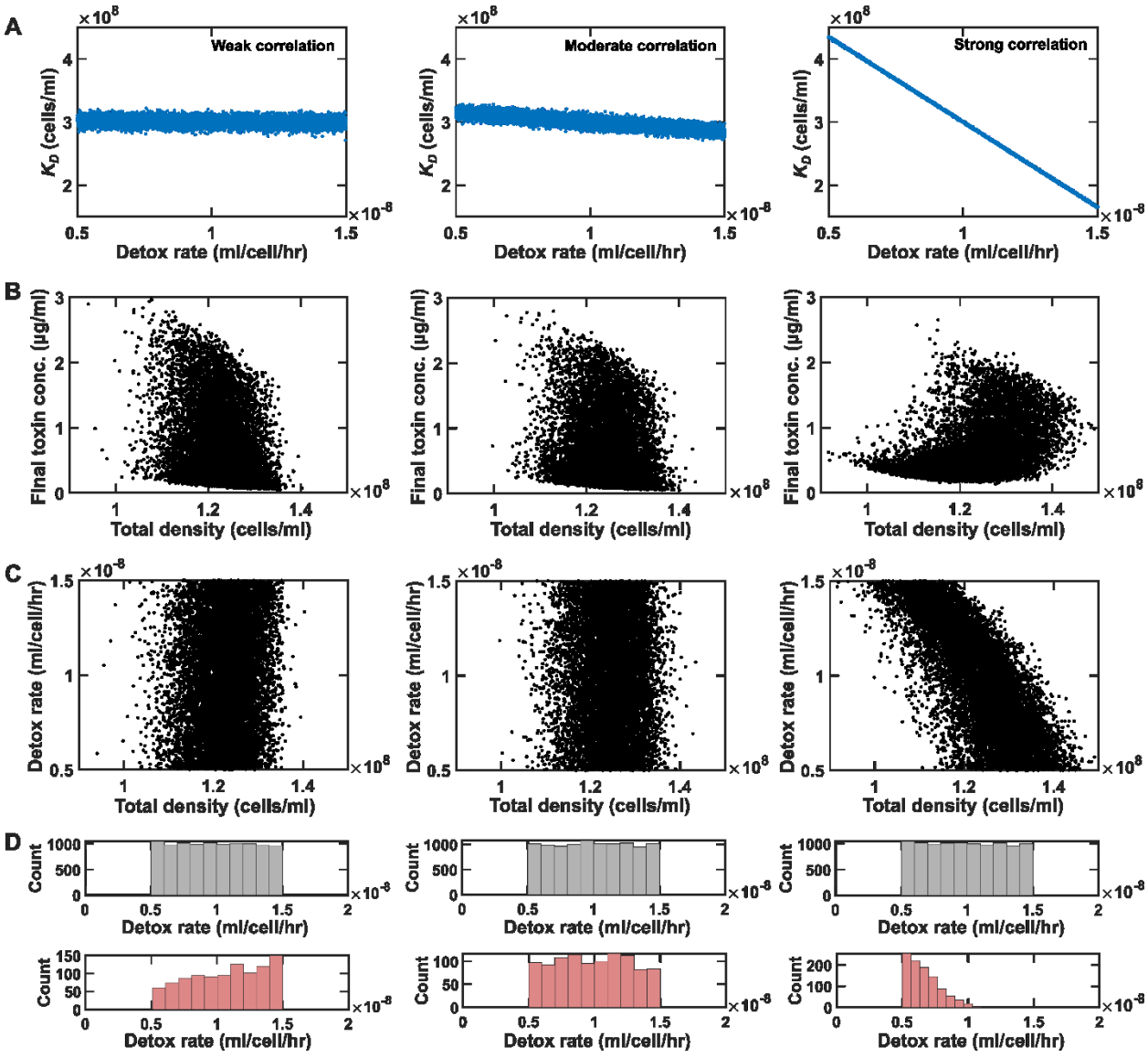

Figure S9. Tradeoff between traits can interfere with detoxification selection, related to Figure 7. We survey n=10000 simulated instances to evaluate how tradeoff in parameters affects PAAS selection. We intentionally introduced tradeoff between K_D and d_D, in the form of $K_D = (1-\varphi)K_{D0} + \varphi K_{Dm}[1-(d_{D0}-d_{Dm})/d_{Dm}]$. Here K_{D0} and d_{D0} are random variables with properties listed in Tables 1 and 2, d_{Dm} is the average value of d_{D0}, and φ is a free parameter that determines the strength of correlation between K_D and d_D in each instance. A.) For φ = 0.01, 0.1, and 0.9, describing examples of weak, intermediate, and strong correlation, respectively, the relation between sampled K_D and d_D values are shown. B.) Total cell density is tightly linked to the effectiveness of detoxification in the weak tradeoff case (φ = 0.01, left) but not in the strong tradeoff case (φ = 0.9, right). C.) Scatter-plot shows a positive correlation between the detoxification rate and total cell density in the weak tradeoff case (φ = 0.01, left) but the correlation turns negative when the tradeoff is strong (φ = 0.9, right). D.) Comparing the distributions of the detoxification rates before selection (top, grey) and after selecting the top 10% instances with the highest total cell densities (bottom, pink) shows that PAAS favors improved detoxification in the weak tradeoff case (φ = 0.01, left) but not when the tradeoff is strong (φ = 0.9, right). Final **T** concentrations are from simulations at 46 hours. The initial toxin concentration is 10 µg/ml. The lmplnt model is used in these simulations.

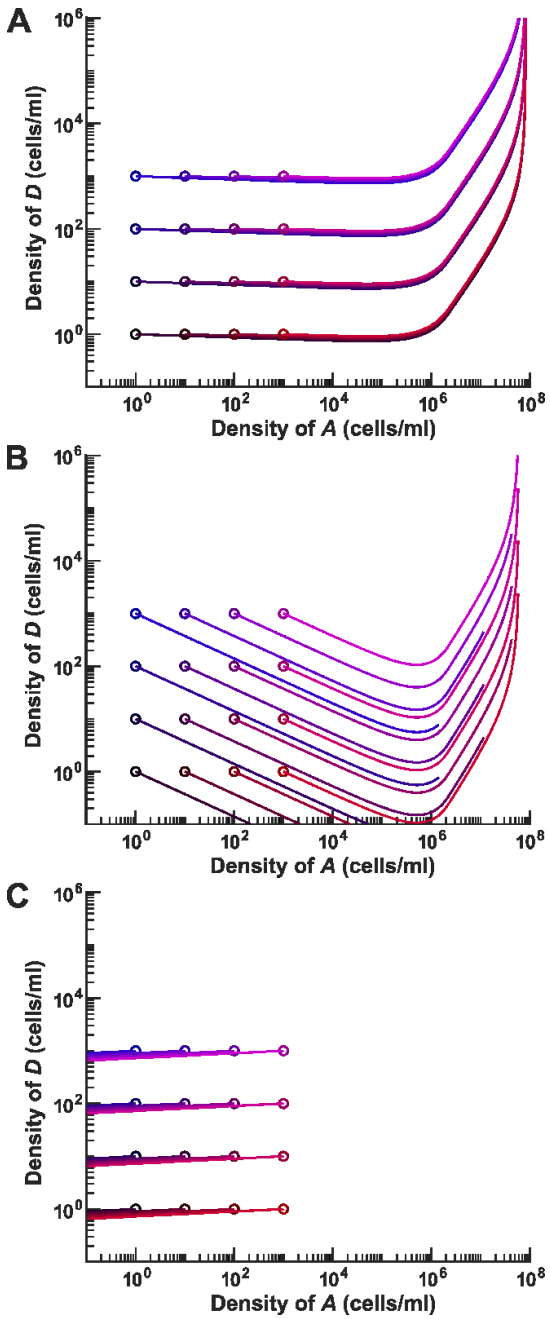

Figure S10. Coculture dynamics is insensitive to the initial ratios of A and D population densities, related to Figure 7. We followed the population dynamics in the two-dimensional space of **A** and **D** densities, starting from a range of initial **A** and **D** densities. Overall, the outcomes appear largely independent of the details of the initial population ratios. A.) With $r_A - \rho_T T_0 > 0$ and small death rates of **A** and **D** (here 0.005/hr), the trajectories of the population dynamics are independent of the initial density of **A**. Additionally, all cases remain viable. B.) With $r_A - \rho_T T_0 > 0$ and at higher death rates of **A** and **D** (here 0.05/hr), lower initial densities of **A** may not be viable (assuming extinction when density of **D** reaches 0.1 cells/ml). This is because **D** goes extinct before **A** grows enough to support it. C.) With $r_A - \rho_T T_0 < 0$, density of **A** declines over time and usability is only possible when the population size of **D** is large enough to detoxify the culture for **A** before **A** goes extinct (not shown here; see "Conditions for Usability"). All parameters are listed in Table 1, with the exception of $\rho_T = 0.03$ ml/(μg·hr) assigned in part (C).